

## Structural Evolution of a Two-Component Organogel

Mohit Singh,<sup>†</sup> Grace Tan,<sup>†</sup> Vivek Agarwal,<sup>‡</sup> Gerhard Fritz,<sup>§</sup> Karol Maskos,<sup>†</sup>  
Arijit Bose,<sup>‡</sup> Vijay John,<sup>\*,†</sup> and Gary McPherson<sup>⊥</sup>

Department of Chemical and Biomolecular Engineering, Tulane University,  
New Orleans, Louisiana 70118; Department of Chemical Engineering,  
University of Rhode Island, Kingston, Rhode Island 02881; Institut für Chemie,  
Karl-Franzens Universität Graz, 8010 Graz, Austria; and Department of Chemistry,  
Tulane University, New Orleans, Louisiana 70118

Received March 9, 2004. In Final Form: May 29, 2004

Dry reverse micelles of AOT in isooctane spontaneously undergo a microstructural transition to an organogel upon the addition of a phenolic dopant, *p*-chlorophenol. This microstructural evolution has been studied through a combination of light scattering, small-angle neutron scattering (SANS), NMR, and rheology. Several equilibrium stages between the system of dry reverse micelles of AOT and a 1:1 AOT/*p*-chlorophenol (molar ratio) gel in isooctane have been examined. To achieve this, *p*-chlorophenol is added progressively to the dilute solutions of AOT in isooctane, and this concentration series is then analyzed. The dry micelles of AOT in isooctane do not undergo any detectable structural change up to a certain *p*-chlorophenol concentration. Upon a very small increment in the concentration of *p*-chlorophenol beyond this "threshold" concentration, large strandlike aggregates are observed which then evolve to the three-dimensional gel network.

### Introduction

Organogels consist of low concentrations of one or more low-molecular-mass organogelators (LMOGs) that self-assemble to form a semirigid three-dimensional network in an organic solvent.<sup>1</sup> These systems constitute an important class of materials due to their applications in templated materials synthesis,<sup>2,3</sup> entrapment of biomolecules,<sup>4</sup> separations,<sup>5</sup> photoinduced charge transfer,<sup>6,7</sup> and biomimetics.<sup>8</sup> The gelation of solvents by small molecules is a consequence of self-assembly into networks where physical interactions mediate cross-links and chain entanglements. The examples of LMOGs in the literature include steroids,<sup>9</sup> organometallic complexes,<sup>10</sup> alkylamide derivatives,<sup>11</sup> and fatty acids.<sup>12</sup> The gelation is dictated by self-assembly through a range of molecular interactions such as hydrogen bonding and  $\pi$ - $\pi$ , hydrophobic, and dispersion interactions. Some recent examples of such systems include the gels of nonpolar solvents with long

chain alkanes reported by Weiss and co-workers,<sup>1,13</sup> the organogels formed by networks of cholesterol linkages with anthracene derivatives also studied by Weiss and co-workers,<sup>14</sup> the cholesterol-azobenzene linkage based gels of Shinkai and co-workers,<sup>15</sup> and the cholesterol-stilbene and cholesterol-squaraine based gels reported by Whitten and co-workers.<sup>16</sup>

Microstructural investigations have been conducted on a variety of organogels in the past.<sup>13,16–18</sup> Several of these reports have been focused on elucidating the microstructure of the organogels well above the percolation threshold. However, the process of gelation is an important problem to address.<sup>19</sup> The recent literature indicates a significant interest in understanding the microstructure of the pregels and the mechanism of the evolution of these pregels (sols) into the corresponding organogels. Wang and co-workers<sup>20</sup> have looked at the role of the solvent-gelator interactions in the formation of cholesterol-stilbene based organogels via in-situ AFM (atomic force microscopy) measurements. The authors have shown that solvent-gelator interaction is an important factor in the formation of the organogel fibers, and the organogel formation takes place through

<sup>†</sup> Department of Chemical and Biomolecular Engineering, Tulane University.

<sup>‡</sup> University of Rhode Island.

<sup>§</sup> Universität Graz.

<sup>⊥</sup> Department of Chemistry, Tulane University.

\* Corresponding author: e-mail vijay.john@tulane.edu.

(1) Abdallah, D. J.; Weiss, R. G. *Adv. Mater.* **2000**, *12*, 1237.

(2) Rees, G. D.; Robinson, B. H. *Adv. Mater.* **1993**, *5*, 608.

(3) Loos, M.; Esch, J.; Stokroos, I.; Kellogg, R. M.; Feringa, B. L. *J. Am. Chem. Soc.* **1997**, *119*, 12675.

(4) Haering, G.; Luisi, P. L. *J. Phys. Chem.* **1986**, *90*, 5892.

(5) Phillips, R. J.; Deen, W. M.; Brady, J. F. *J. Colloid Interface Sci.* **1990**, *139*, 363.

(6) Ajayaghosh, A.; George, S. J.; Praveen, V. K. *Angew. Chem.* **2003**, *42*, 332.

(7) Shirakawa, M.; Fujita, N.; Shinkai, S. *J. Am. Chem. Soc.* **2003**, *125*, 9902.

(8) Hafkamp, R. J. H.; Kokke, P. A.; Danke, I. M.; Guerts, H. P. M.; Rowan, A. E.; Feiters, M. C.; Nolte, R. J. M. *Chem. Commun.* **1997**, 545.

(9) Terech, P.; Ramasseul, R.; Volino, F. *J. Phys. (Paris)* **1985**, *46*, 895.

(10) Terech, P.; Chachaty, C.; Gaillard, J.; Giroud-Godquin, A. M. *J. Phys. (Paris)* **1987**, *48*, 663.

(11) Hanabusa, K.; Tange, J.; Taguchi, Y.; Koyama, T.; Shirai, H. *J. Chem. Soc., Chem. Commun.* **1993**, 390.

(12) Tachibana, T.; Mori, T.; Hori, K. *Bull. Chem. Soc. Jpn.* **1980**, *53*, 1714.

(13) (a) Abdallah, D. J.; Weiss, R. G. *Langmuir* **2000**, *16*, 352. (b) Abdallah, D. J.; Sirchio, S. A.; Weiss, R. G. *Langmuir* **2000**, *16*, 7558.

(14) (a) Lin, Y. C.; Kachar, B.; Weiss, R. G. *J. Am. Chem. Soc.* **1989**, *111*, 5542. (b) Terech, P.; Furman, I.; Weiss, R. G. *J. Phys. Chem.* **1995**, *99*, 9558. (c) Terech, P.; Ostuni, E.; Weiss, R. G. *J. Phys. Chem.* **1996**, *100*, 3759.

(15) Murata, K.; Aoki, M.; Suzuki, T.; Harada, T.; Kawabata, H.; Komori, T.; Ohseto, F.; Ueda, K.; Shinkai, S. *J. Am. Chem. Soc.* **1994**, *116*, 6664.

(16) (a) Geiger, C.; Stanesco, M.; Chen, L.; Whitten, D. G. *Langmuir* **1999**, *15*, 2241. (b) Duncan, D.; Whitten, D. G. *Langmuir* **2000**, *16*, 6445.

(17) (a) Terech, P.; Coutin, A.; Giroud-Godquin, A. M. *J. Phys. Chem. B* **1997**, *101*, 6810. (b) Terech, P.; Allegraud, J. J.; Garner, C. M. *Langmuir* **1998**, *14*, 3991. (c) Terech, P.; Meerschaut, D.; Desvergne, J.-P.; Colomes, M.; Bouas-Laurent, H. *J. Colloid Interface Sci.* **2003**, *261*, 441.

(18) Schmidt, R.; Schmutz, M.; Mathis, A.; Decher, G.; Rawiso, M.; Mesini, P. *J. Langmuir* **2002**, *18*, 7167.

(19) Lescanne, M.; Colin, A.; Mondain-Monval, O.; Fages, F.; Pozzo, J.-L. *Langmuir* **2003**, *19*, 2013.

(20) Wang, R.; Geiger, C.; Chen, L.; Swanson, B.; Whitten, D. G. *J. Am. Chem. Soc.* **2000**, *122*, 2399.

a phase separation in the precursor sol and subsequent fibril growth. Recently, Sakurai and co-workers<sup>21</sup> have also reported a similar mechanism by time-resolved SAXS (small-angle X-ray scattering) measurements on a sugar-based organogel. Liu and co-workers<sup>22</sup> have used in-situ rheological measurements, light scattering, and supercritical fluid CO<sub>2</sub> extraction/SEM (scanning electron microscopy) to elucidate the formation of a nano-fiber network in a *N*-lauroyl-L-glutamic acid di-*n*-butylamide organogel in isostearyl alcohol and indicated a nucleation-growth-noncrystallographic branching mechanism. Lescanne and co-workers<sup>23</sup> have investigated the mechanism of the formation of an organogel of the gelator 2,3-di-*n*-decyloxyanthracene (DDOA) in propylene carbonate using light microscopy, light and X-ray scattering, and rheological measurements. The authors have suggested that the gel formation is due to a precipitation process that occurs via a nucleation-growth mechanism. Wilder and co-workers<sup>24</sup> have studied the in-situ dynamic rheological response during the formation of dibenzylidene sorbitol (DBS) organogels in poly(ethylene glycol) (PEG) and PEG derivatives. The dynamic rheological measurements indicate that the rate of growth of the elastic moduli is sensitive to the DBS concentration and the matrix polarity.

We have previously reported that a novel class of organogels is formed when acidic (low *pK<sub>a</sub>*) phenolic compounds, such as *p*-chlorophenol, are added to anhydrous solutions of the anionic twin-tailed surfactant bis-(2-ethylhexyl) sodium sulfosuccinate (AOT) and a nonpolar solvent.<sup>25–27</sup> These organogels are most stable when the phenol to AOT molar ratio is close to unity. Typically, AOT in nonpolar solvents forms spherical inverse micelles. Upon addition of the phenolic component, the low-viscosity micellar solution spontaneously transforms into a rigid organogel. The organogels have a sharp melting point and also break down when exposed to trace amounts of moisture. Our previous studies using FTIR spectroscopy have indicated that hydrogen-bonding interactions between the phenol and the sulfosuccinate headgroup of AOT appear to be the driving forces for gelation.<sup>25–27</sup> Small-angle X-ray scattering (SAXS) and atomic force microscopy (AFM) investigations of the gel system in its native state reveal that the system self-assembles to fibers that aggregate to fiber bundles.<sup>28</sup>

The organogel formation in the AOT/*p*-chlorophenol system results from the interactions between two small molecules (LMOGs), where one of the components (AOT) self-assembles (in the absence of *p*-chlorophenol) into spherical reverse micelles in the solvent (isooctane). The organogel evolves as *p*-chlorophenol is progressively added to this AOT micellar solution in isooctane. This makes this system distinct from single gelator based organogels studied in the literature<sup>20–24</sup> and an interesting candidate for a systematic analysis, where we can focus on the

Table 1. Sample Descriptions

sample ID	[AOT] (M)	[ClPh] (M)	physical appearance
S1	0	0	clear solvent
S2	0.02	0	clear solution
S3	0.04	0	clear solution
S4	0.02	0.0025	clear solution
S5	0.02	0.005	clear solution
S6	0.02	0.00525	clear solution
S7	0.02	0.0055	clear solution
S8	0.02	0.006	turbid clusters in liquid
S9	0.02	0.01	opaque gel
S10	0.02	0.02	opaque gel

evolution of the system from reverse micelles of the surfactant AOT to an organogel with a three-dimensional network, upon incremental addition of the phenol. A widely studied class of organogels based on AOT/isooctane microemulsions is the four-component system water/AOT/isooctane/gelatin where gelatin (MW ~ 200, 000) acts as the gelator.<sup>29</sup> The formation of this four-component organogel is understood in terms of the percolation of the AOT microemulsion droplets, facilitated by the bridging by gelatin strands (~100 nm) swollen with water.<sup>29</sup> The interesting aspect of our system that makes it very different from the quaternary organogel system based on water/AOT/isooctane/gelatin is self-assembly based on small gelator molecules (*p*-chlorophenol) in the absence of water, which has a strong destabilizing effect on gelation.<sup>28</sup> In the present work, we investigate this microstructural evolution through a combination of light scattering, small-angle neutron scattering (SANS), NMR, and rheology. The mechanism involved in the evolution of the three-dimensional gel network provides an insight into the interactions that lead to gelation and growth of the three-dimensional network. This may provide a better predictability and control over the final microstructure of the self-assembled microstructure.

## Experimental Section

**Materials and Sample Preparation.** All chemicals were purchased from Aldrich as analytical grade quality reagents and used as received. To remove any trace water from sodium bis-(2-ethylhexyl) sulfosuccinate (AOT), it was dried in a vacuum oven at 80 °C for 10 h before use. Reverse micellar solutions of AOT were prepared by dissolving a measured amount of AOT in isooctane. Organogel samples were prepared by adding varying amounts of *p*-chlorophenol to the AOT reverse micellar solution. Table 1 provides the sample details for the entire series. Typically, pregel mixtures, contained in 20 mL capped vials to prevent water absorption from the ambient air, were heated at 40–70 °C in a warm water bath and sonicated until all components were dissolved as evidenced by a clear isotropic solution. The mixtures were then removed from the water bath and allowed to cool. The organogel samples below a certain concentration of *p*-chlorophenol were clear isotropic solutions after cooling. The samples beyond this concentration show varying levels of turbidity at room temperature.

**Light Scattering.** Light scattering was performed on a Coulter model N4 MD submicron particle analyzer. The scattered intensity was measured at 90° from the direction of the incident beam. Liquid samples were prepared with filtered stock solutions. These samples were pipetted into a quartz cell and allowed to equilibrate for 15 min before analysis. Gel samples were heated to form homogeneous solutions before they were transferred into

(21) Sakurai, K.; Jeong, Y.; Koumoto, K.; Friggeri, A.; Gronwald, O.; Sakurai, S.; Okamoto, S.; Inoue, K.; Shinkai, S. *Langmuir* **2003**, *19*, 8211.

(22) Liu, X. Y.; Sawant, P. D. *Appl. Phys. Lett.* **2001**, *79*, 3518.

(23) Lescanne, M.; Colin, A.; Mondain-Monval, O.; Fages, F.; Pozzo, J.-L. *Langmuir* **2003**, *19*, 2013.

(24) Wilder, E. A.; Hall, C. K.; Khan, S. A.; Spontak, R. J. *Langmuir* **2003**, *19*, 6004.

(25) Xu, X.; Ayyagari, M.; Tata, M.; John, V. T.; McPherson, G. L. *J. Phys. Chem.* **1993**, *97*, 11350.

(26) Tata, M.; John, V. T.; Waguespack, Y. Y.; McPherson, G. L. *J. Am. Chem. Soc.* **1994**, *116*, 9464.

(27) Tata, M.; John, V. T.; Waguespack, Y. Y.; McPherson, G. L. *J. Phys. Chem.* **1994**, *98*, 3809.

(28) Simmons, B. A.; Taylor, C. E.; Landis, F. A.; John, V. T.; McPherson, G. L.; Schwartz, D. K.; Moore, R. *J. Am. Chem. Soc.* **2001**, *123*, 2414.

(29) Greener, J.; Contestable, B. A.; Bale, M. D. *Macromolecules* **1987**, *20*, 2490. Capitani, D.; Segre, A. L.; Haering, G.; Luisi, P. L. *J. Phys. Chem.* **1988**, *92*, 3500. Atkinson, P. J.; Grimson, M. J.; Heenan, R. K.; Howe, A. M.; Mackie, A. R.; Robinson, B. H. *Chem. Phys. Lett.* **1988**, *151*, 494. Quellet, C.; Eicke, H. F.; Sager, W. *J. Phys. Chem.* **1991**, *95*, 5642. Petit, C.; Zemb, T.; Pileni, M. P. *Langmuir* **1991**, *7*, 223. Atkinson, P. J.; Robinson, B. H.; Howe, A. M.; Pitt, A. R. *Colloids Surf., A* **1995**, *94*, 231. Caldararu, H.; Timmins, G. S.; Gilbert, B. C. *Phys. Chem. Chem. Phys.* **1999**, *1*, 5689.

the quartz cell and allowed to cool before analysis. Three readings were taken per sample over a scan period of 5 min each.

**SANS.** SANS measurements were carried out on the 30 m NG3 beamline at the NIST Center for Neutron Research (NCNR), Gaithersburg, MD. The instrument utilizes a mechanical velocity selector as a monochromator, a circular pinhole collimator, and a two-dimensional position-sensitive detector ( $65 \times 65 \text{ cm}^2$ ). The SANS intensity,  $I$ , was recorded as a function of the magnitude of the scattering vector,  $q = (4\pi/\lambda) \sin(\theta/2)$ , where  $\theta$  is the scattering angle and  $\lambda$  is the neutron wavelength (equal to 6 Å). The detector angle was set at  $2^\circ$ , and the sample-to-detector distance was set to 2 and 13 m to cover the widest possible range of  $q$  ( $0.004\text{--}0.6 \text{ \AA}^{-1}$ ). Samples were contained in closed stainless steel cells with quartz windows that provided a path length of 2 mm. The sample temperature was maintained at  $25^\circ\text{C}$ . The raw data were corrected for scattering from an empty quartz cell, the detector sensitivity and background, and the transmission of each sample and were placed on an absolute scale using software provided by NCNR. The primary component in our microemulsion/organogel system is *d*-isooctane. The scattering data were plotted as  $I(q) - B$ , where  $I(q)$  is the total scattered intensity and  $B$  is the background calculated from the slope of a Porod plot ( $Iq^4$  vs  $q^4$ ).

**Light Microscopy.** Light microscopy images were obtained using a Leica DM IRE2 inverted microscope. A drop of the sample was placed on a clean microscopic glass slide and covered with a cover glass, and the sides of the cover glass were sealed with grease to prevent solvent evaporation.

**NMR.** NMR measurements were performed at  $25^\circ\text{C}$  on a Bruker DRX 500 MHz NMR spectrometer. All samples for NMR were prepared with spectrometric grade isooctane.

**Rheological Experiments.** Rheological tests were conducted on a TA Instruments AR-2000 constant stress (controlled strain and controlled rate are achieved through an extremely sensitive feed back loop) rheometer with a built-in temperature and gap calibration. A double concentric cylinder geometry was used as the organogel samples at low *p*-chlorophenol concentrations have a very low viscosity. A vendor supplied solvent trap was used to mitigate solvent loss from the system. Both steady shear and oscillatory shear experiments were performed in stress-controlled mode. The linear viscoelastic limit for the samples subjected to oscillatory shear was determined through stress sweep experiments.

### SANS Data Analysis

Two approaches for analyzing the small-angle neutron scattering (SANS) data from micellar systems involve fitting the experimental data to a known scattering model or the use of a model-free approach.<sup>30</sup> The first approach is to compare the scattering data to calculated scattering curves of model structures. The limitation of the model-fitting approach is that multiple models can sometimes describe a set of SANS data through parameter adjustments, making it very difficult to find the correct model without any a priori knowledge about the scattering system.

The analysis of SANS data presented here deals with the second approach, in particular, a technique called generalized indirect Fourier transformation (GIFT) developed by Glatter and co-workers.<sup>31</sup> Generally, this procedure is preferred if there is insufficient information to make any a priori assumption, especially if the scattering entities interact. The scattering intensity  $I(q)$  at different scattering vectors  $\mathbf{q}$  is only a function of shape, size, and internal structure for noninteracting particles. In the case of interacting particles the intensity does not depend solely on these parameters. Neighboring particles can influence the scattering curve considerably, leading

to interparticle effects represented by the so-called structure factor  $S(q)$ , while the intraparticle effects are described by the form factor  $P(q)$ . In the case of  $N$  monodisperse, homogeneous, globular, interacting particles, the total scattering intensity can be expressed by

$$I(q) = NP(q) S(q) \quad (1)$$

This factorization allows a separation of inter- and intraparticle effects by means of the generalized indirect Fourier transformation (GIFT) technique. For a particle of arbitrary shape, the pair distance distribution function (PDDF),  $p(r)$ , is given by

$$p(r) = r^2 \Delta \bar{\rho}^2(r) \quad (2)$$

where  $\Delta \bar{\rho}^2(r)$  is the convolution square of  $\Delta \rho(r)$ , the scattering density difference, averaged over all directions. The PDDF is related to the scattered intensity  $I(q)$  through the form factor  $P(q)$  by the Fourier transformation

$$P(q) = 4\pi \int_0^\infty p(r) \frac{\sin(qr)}{qr} dr \quad (3)$$

The GIFT method approximates the form factor, represented by a linear combination of a finite number of cubic B-spline functions. At the same time, a model for the structure factor is assumed and fitted to the data according to eq 1. This simultaneous approximation of form and structure factor is only possible due to the different mathematical properties of the two functions. Nevertheless, the problem is now highly nonlinear and has to be solved in an iterative way. Fritz and co-workers<sup>32</sup> have explained the steps involved in this GIFT calculation in a detailed and well-structured manner.

The shape of the PDDF offers a fair idea of the basic geometry such as spherical, cylindrical, and lamellar, even for inhomogeneous particles. Knowledge of  $p(r)$  also excludes certain structural alternatives. After the PDDF is determined, a cross-sectional  $p(r)$  of cylindrical or flat structures can be obtained by using the symmetry obtained in the first step. This cross-sectional  $p(r)$  provides further information about the cross-sectional shape and size of the scattering entities.

Strictly speaking, the factorization into a form factor and a structure factor is only possible for spherical particles due to orientation correlations.<sup>32</sup> As stated, a model for the structure factor has to be assumed for use in the GIFT technique. In the present study the modified Ornstein–Zernike relation<sup>33</sup>

$$S(q) = 1 + \frac{S(0)}{1 + (q\xi)^2} \quad (4)$$

has been used for structure factor calculations. Here,  $S(0) = \rho k_B TK$ , where  $k_B$  is the Boltzmann constant and  $T$  is the temperature.  $K$  is the isothermal compressibility, and  $\xi$  is the correlation length of the critical fluctuations. This structure factor model had been shown to work well for water-in-oil microemulsions<sup>34</sup> and nonionic micelles.<sup>35</sup>

(32) Fritz, G.; Bergmann, A.; Glatter, O. *J. Chem. Phys.* **2000**, *113*, 9733.

(33) Chen, S.-H. *Annu. Rev. Phys. Chem.* **1986**, *37*, 351.

(34) Kaler, E. W.; Billman, J. F.; Fulton, J. L.; Smith, R. D. *J. Phys. Chem.* **1991**, *95*, 458.

(35) Glatter, O.; Fritz, G.; Lindner, H.; Popela, J. B.; Mittelbach, R.; Strey, R.; Egelhaaf, S. U. *Langmuir* **2000**, *16*, 8692.

(30) Glatter, O. *J. Appl. Crystallogr.* **1977**, *10*, 415.

(31) (a) Glatter, O. *J. Appl. Crystallogr.* **1981**, *14*, 577. (b) Glatter, O.; Hainisch, B. *J. Appl. Crystallogr.* **1984**, *17*, 435. (c) Glatter, O. *J. Appl. Crystallogr.* **1988**, *21*, 886.

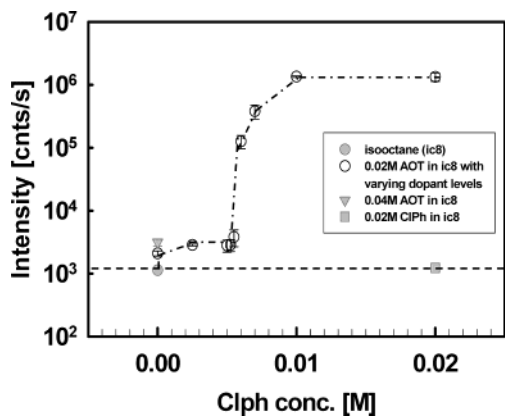


**Figure 1.** Light scattering intensity at various *p*-chlorophenol concentrations (S1–S10).

### Results and Discussion

Table 1 provides a description of all samples used in the study. Figure 1 illustrates the light scattering results of these samples. The total intensity of the scattered light from a solution/suspension of noninteracting particles is proportional to the difference in the refractive indices of the particles and the solvent and the size of the scattering entities.<sup>36</sup> When the particles interact, the total scattered intensity is affected due to interparticle interactions.<sup>37</sup> For the organogel series investigated in the present work, the difference in the refractive indices between the scattering entities (micelles) and the solvent (isooctane) does not change appreciably. The difference in the total intensity of the scattered light, therefore, may arise from the difference in the sizes of the scattering entities or intermicellar interactions, if they exist. Figure 1 illustrates the total light scattering intensity for the organogel series. The total scattering intensity levels for the solvent (isooctane) and 0.02 M *p*-chlorophenol solution are virtually identical and serve as the reference level for the remaining samples. The total scattered intensity is higher for the 0.02 M AOT micellar solution due to the presence of AOT micelles. The scattered intensity shows a slight increase as *p*-chlorophenol is progressively added to the 0.02 M AOT micellar solutions because of a monotonic increase in the optical contrast upon adding *p*-chlorophenol. A dramatic change in the scattering intensity is seen as the concentration of *p*-chlorophenol is increased from 0.0055 M (S7) to 0.006 M (S8). For sample S8, a few translucent clusters are visibly detected in the solution. This indicates the formation of large aggregates in the organogel system beyond a threshold *p*-chlorophenol concentration.

SANS experiments were performed on the entire series (S2–S10) of samples to further elucidate the effect of *p*-chlorophenol doping on the AOT micelles. Figure 2a illustrates the SANS data corresponding to the entire doping series. The symbols represent the experimental data, and the solid lines represent the corresponding GIFT approximations. For samples S2–S7, the GIFT approximations follow the experimental data with a high accuracy of <5% deviation from all experimental data points. The GIFT approximations corresponding to the samples at higher *p*-chlorophenol concentrations (S8–S10) are not shown, as a low mean deviation could not be obtained for these samples.

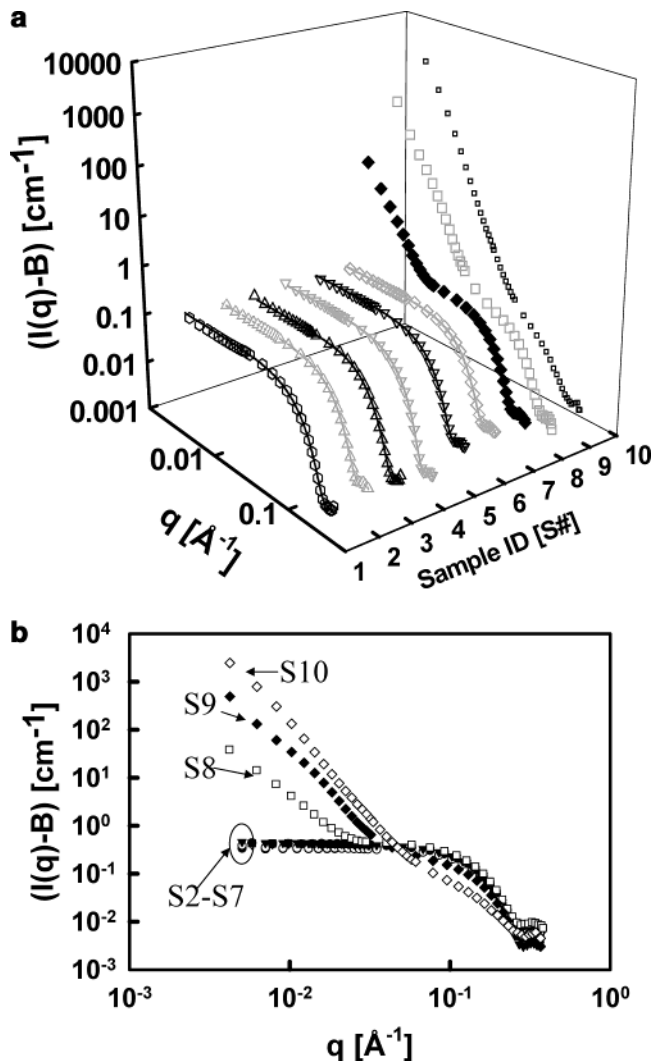


**Figure 2.** (a) Small-angle neutron scattering (SANS) profiles for AOT micelles doped with varying concentrations of *p*-chlorophenol (symbols). The solid lines for samples S2–S7 show the corresponding GIFT approximations. (b) Two-dimensional representations of the SANS profiles.

The SANS data for the samples S2–S7 follow a very similar trend. The PDDFs obtained through the GIFT (IFT, as the structure factor is equal to 1 in samples S2–S7) analysis of the data for samples S2–S7 indicate that the shape and size of the scattering entities present in the system remains essentially unchanged (Figure 3). The highly symmetric shape of these PDDFs indicates that the scattering entities are globular.<sup>31</sup> The size of these scattering entities (micelles) present in the control samples S2 (0.02 M AOT) and S3 (0.04 M AOT) is approximately 3.2 nm. Additionally, the scattering data of sample S3 indicate that structure factor effects are not observed, clearly indicating negligible intermicellar interactions when the concentration of AOT is doubled from that of sample S2. This observation points to the fact that the gel formation at 1:1 AOT/ *p*-chlorophenol molar ratio (corresponding to a total gelator concentration of 0.04 M in the solvent) is not a simple excluded-volume effect but is a result of the synergy between the two components. The value of the micellar size is in a good agreement with the size of AOT reverse micelles in isooctane<sup>36</sup> and decane,<sup>38</sup>

(36) Zulaf, M.; Eicke, H.-F. *J. Phys. Chem.* **1979**, *83*, 480.

(37) Brunetti, S.; Roux, D.; Belloq, A. M.; Bothorel, P. *J. Phys. Chem.* **1983**, *87*, 1028.

(38) Kotlarchyk, M.; Huang, J. S.; Chen, S.-H. *J. Phys. Chem.* **1985**, *89*, 4382.

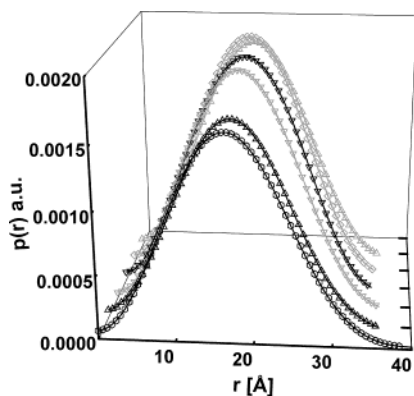
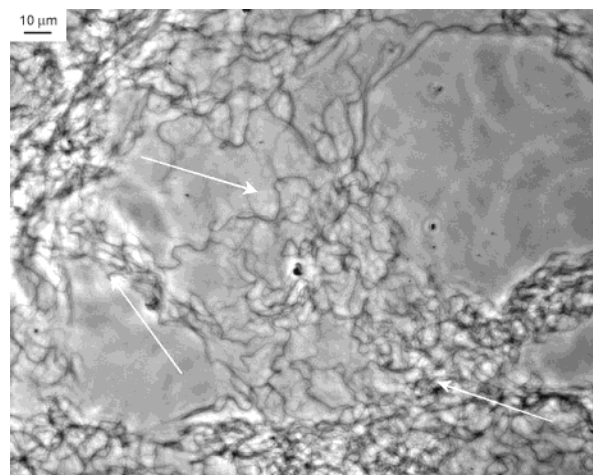


**Figure 3.** Pair density distribution functions (PDDF) for AOT micelles doped with varying concentrations of *p*-chlorophenol (samples S2–S7 moving from the front to the back).

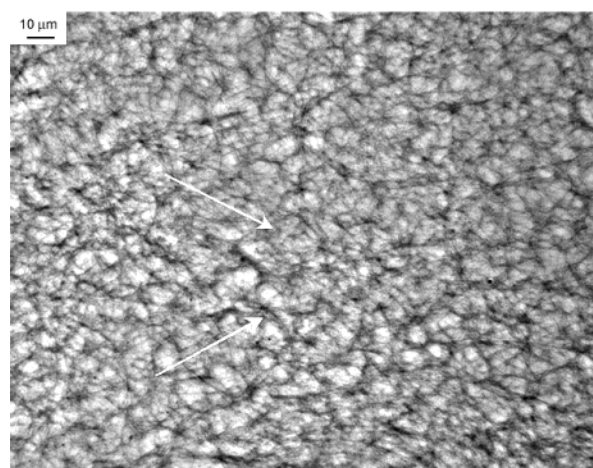
reported in the literature. The size and the shape of the scattering entities do not change with increasing *p*-chlorophenol doping (sample S4–S7). At higher concentrations of *p*-chlorophenol (S8–S10), the structure factor effects are too severe to allow GIFT calculation with a low mean deviation. The PDDFs corresponding to these data cannot be determined uniquely using GIFT calculations. However, the enhanced low-angle scattering (S8–S10, Figure 2a,b) suggests the presence of large scattering entities (aggregates). Also, in the high- $q$  region ( $q \sim 0.1 \text{ \AA}^{-1}$ ), these data follow a trend very similar to that of samples S2–S7 (Figure 2b). This indicates that the large aggregates present in the system possess an internal structure on the same scale as that of micelles. Thus, the SANS data indicate a very sharp transition (S7 to S8) from globular micelles to large structured aggregates upon increasing *p*-chlorophenol concentration. Although it is tempting to say the aggregates at least initially retain the globular microstructure of reverse micelles (sample S8), we are unable to use GIFT to make distinctions between globular and rod-shaped structures through the shape of the PDDFs. This plausible explanation in terms of the percolation of globular reverse micelles is similar to the percolation phenomenon postulated in the water/AOT/isooctane/gelatin four-component organogel that has been studied extensively in the literature.<sup>29</sup> What we do know, however, is that as the gel sets (samples S9 and 10), X-ray diffraction data imply aggregation of strands to hexagonally ordered fibers.<sup>28</sup>

As the extent of *p*-chlorophenol doping increases beyond sample S7 to sample S8, translucent cluster-like entities are visually observed. Optical microscopy (Figure 4) reveals that these clusters are entangled fibers, with solvent filling up the space between the fibers. Sample S8 is composed of several of these clusters. These clusters have a poor intraconnectivity, as observed in Figure 4a. The poor connectivity between and within these clusters prevents them from effectively immobilizing the solvent completely to form a gel. When more *p*-chlorophenol is added to the sample such that a gel is formed (sample S9), a highly entangled and extremely dense fibrous network is observed (Figure 4b). High resolution atomic force microscopy images of these fibers presented in an earlier study indicate levels of assembly from fiber-type structures to fiber bundles.<sup>28</sup>

We have also carried out  $^1\text{H}$  NMR studies for the organogel series (S2–S10) to understand these micelles/aggregates at the molecular level.  $^1\text{H}$  NMR studies have been used extensively in the field of organogels to elucidate the molecular interactions responsible for self-assembly



(a)



(b)

**Figure 4.** (a) Optical microscopy image of a cluster in 0.02 M AOT/0.006 M *p*-chlorophenol (sample S8) in isooctane. The arrows show the loosely connected strands/fibers. (b) Optical microscopy image of the 0.02 M AOT/0.01 M *p*-chlorophenol (sample S9) in isooctane. The arrows show the entangled strands/fibers and the junction points.

and network formation.<sup>26,39</sup> We have examined the  $^1\text{H}$  resonances of both organogel components, AOT and *p*-chlorophenol. The NMR spectra for *p*-chlorophenol in the solvent (isooctane) and the organogel system are illustrated in Figure 5a. Figure 5b illustrates the peak positions for the *p*-chlorophenol protons for the entire concentration series (S2–S10). When *p*-chlorophenol is dissolved in isooctane in the absence of AOT, the peak corresponding to the hydroxyl proton is broadened due to hydrogen bonding between the *p*-chlorophenol molecules and is not visible in the spectra. As soon as AOT is added to the *p*-chlorophenol solution in isooctane, the peak corresponding to the hydroxyl proton is visible, and the difference between the chemical shifts of the ortho and meta protons of *p*-chlorophenol is reduced (Figure 5a,b). This indicates that *p*-chlorophenol molecules prefer to hydrogen bond with AOT molecules that exist as reverse micelles in isooctane. This is a clear evidence of an interaction between AOT and *p*-chlorophenol molecules at very low *p*-chlorophenol concentrations, even before any clusters are evident in the system. There is no dramatic change in the spectra for *p*-chlorophenol when

(39) Duncan, D.; Whitten, D. G. *Langmuir* **2000**, *16*, 6445.

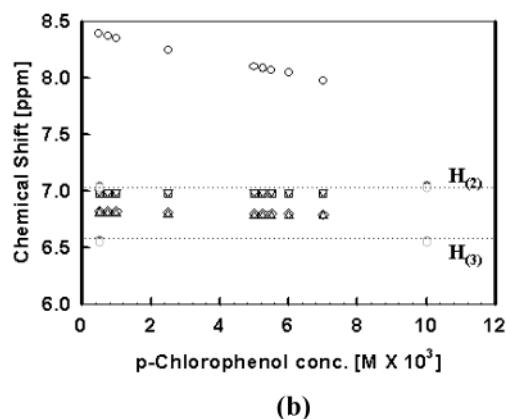
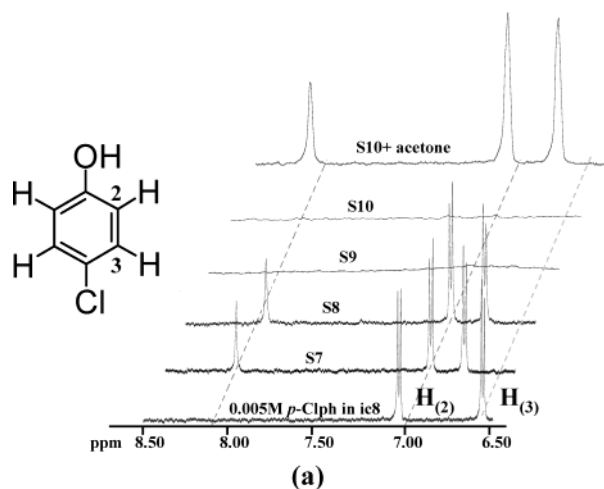


**Figure 5.** (a) NMR spectra for *p*-chlorophenol in the solvent (isooctane) and the AOT/*p*-chlorophenol organogel system. The last spectrum is obtained after adding a trace amount of acetone to the organogel sample S10. The structure of the dopant, *p*-chlorophenol, is also indicated. 2 and 3 are ortho and meta protons of *p*-chlorophenol with respect to the hydroxyl group. (b) Chemical shift of the *p*-chlorophenol protons as a function of its concentration (black symbols) in 0.02 M AOT/isooctane solution. The gray symbols represent the chemical shifts for the *p*-chlorophenol protons at two concentrations in isooctane.

clusters become observable (sample S8, Figure 5a,b). But on transformation to the gel (samples S9 and S10), the peaks corresponding to the ortho and meta protons on *p*-chlorophenol undergo significant line broadening (Figure 5a). This suggests that the *p*-chlorophenol molecules that were “labile” on the NMR time scale when in clusters become “rigid” upon the formation of a three-dimensional network.<sup>26</sup> The observation further supports the formation of a rigid network above the percolation threshold (sample S9). When a trace amount of acetone is added to sample S10 (which is a rigid gel), the gel breaks down into a low-viscosity liquid, and the peak corresponding to the hydroxyl proton reemerges (Figure 5a). This reiterates the importance of hydrogen bonding between AOT and *p*-chlorophenol in the formation of the organogel. The gel breaks down as acetone molecules compete with AOT molecules in forming hydrogen bonds with *p*-chlorophenol.

The rheological response of a micellar system is a function of both microstructure and micelle volume fraction.<sup>40</sup> Steady shear and dynamic rheological measurements were performed on the organogel series (S1–S10). The volume fraction of the micelles in the 0.02 M

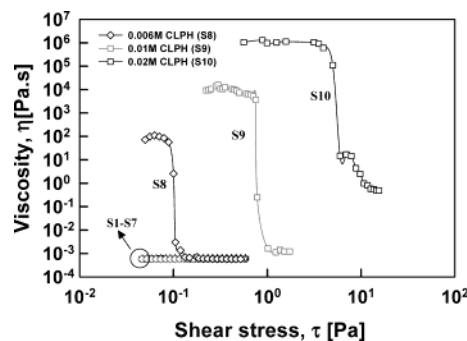


**Figure 6.** Steady shear viscosity ( $\eta$ ) as a function of shear stress ( $\tau$ ) for the samples S1–S10.

AOT micellar system is very small (<1%). This volume fraction does not change appreciably upon the progressive addition of *p*-chlorophenol. Figure 6 illustrates the rheological response of the organogel series upon application of steady shear. Samples S2–S7 indicate Newtonian behavior, with viscosities close to the solvent (isooctane-S1) viscosity. This observation is consistent with the light scattering and SANS data, indicating that the micellar size or shape does not change appreciably upon *p*-chlorophenol doping. Samples S8–S10 show a shear thinning behavior (Figure 6). Sample S8 is the first sample in the concentration series (S1–S10) where large aggregates, visible under an optical microscope, are present. These aggregates break down upon the application of shear, and at high shear stress values (or shear rates), the viscosity of the sample (S8) is very close to the viscosity of samples containing globular micelles in solution (S2–S7). Sample S9 is the first gel sample in the series. This sample also shows a shear thinning behavior, but the viscosity in the high shear rate region is a little higher than in samples S1–S8 (Figure 6). The organogel sample S10 follows a similar trend, only with a larger high shear viscosity. There is a systematic increase in the low shear viscosities from samples S7–S10, indicating an evolution of a network in the system at higher *p*-chlorophenol levels. This information is also reflected in the dynamic (viscoelastic) response of samples S8–S10. Figure 7 shows the viscoelastic response of these samples. Sample S8 shows a rheological behavior typical of networks that are close to the gelation threshold (Figure 7a). The two main features of this behavior are (i) the elastic modulus ( $G'$ ) is lower than the loss modulus ( $G''$ ) for the range of frequencies scanned over and (ii) the dynamic moduli ( $G'$ ,  $G''$ ) show an exponential dependence on the oscillation frequency ( $\omega$ ).<sup>41</sup> The power law behavior for the dynamic moduli ( $G'(\omega) \sim \omega^n \sim G''(\omega)$ ) observed here has been associated with near-critical gels.<sup>42,43</sup> The exponent  $n$  in this case (S8) is 0.78, very close to the predictions ( $n = 0.66$ ) based on Rouse theory for fractal clusters.<sup>44</sup> These data are consistent with the microstructure of sample S8 observed through optical microscopy, where a network of fibers is seen with poor connectivity and dangling ends (Figure 4a). The dynamic response of the gel samples (S9, S10) is shown in Figure 7b. The dynamic moduli do not cross over, and the elastic moduli are always much larger than the loss moduli and almost independent of the oscillation frequency ( $\omega$ ), in the frequency range scanned. This indicates that

(41) Chambon, F.; Winter, H. H. *J. Rheol.* **1987**, *31*, 683.

(42) Chambon, F.; Petrovic, Z. S.; MacKnight, W. J.; Winter, H. H. *Macromolecules* **1986**, *19*, 2146.

(43) Izuka, A.; Winter, H. H.; Hashimoto, T. *Macromolecules* **1992**, *25*, 2422.

(44) Martin, J. E.; Adolf, D.; Wilcoxon, J. P. *Phys. Rev. A* **1989**, *39*, 1325.

(40) Larson, R. G. *The Structure and Rheology of Complex Fluids*; Oxford University Press: Oxford, 1999.

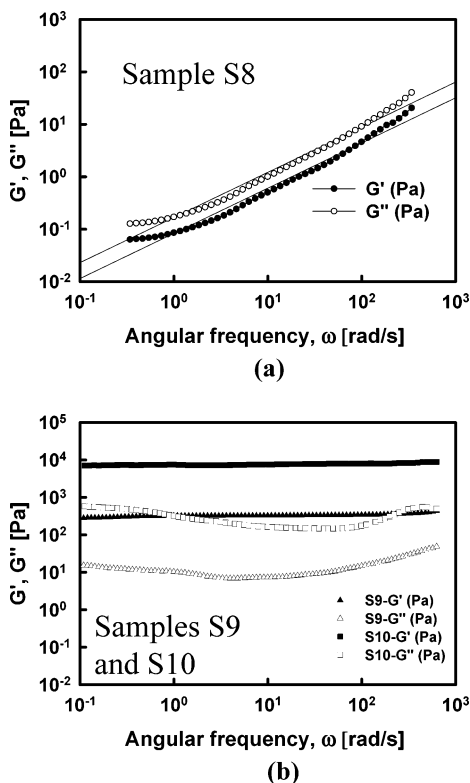


**Figure 7.** (a) Linear viscoelastic response of sample S8. The dynamic moduli ( $G'$ ,  $G''$ ) are measured at a range of frequencies (0.1–500 rad/s). The solid lines indicate the power law behavior. (b) Linear viscoelastic response of samples S9 and S10. The dynamic moduli ( $G'$ ,  $G''$ ) are measured for a range of frequencies (0.1–500 rad/s).

the relaxation times for these gels networks are very large (at least  $>100$  s). Also, the elastic moduli are almost independent of the oscillation frequency ( $\omega$ ) in the frequency range scanned, a behavior typical of solids and highly cross-linked/entangled polymeric systems.<sup>40,45</sup> Again, the data are in agreement with the microstructure of the gel observed through optical microscopy (Figure 4b) where a dense, highly entangled network is seen.

### Summary

The microstructural transitions involved in the formation of a three-dimensional organogel network have been investigated. The organogel is formed due to the interaction and self-assembly of two small molecules, AOT and *p*-chlorophenol, when *p*-chlorophenol is added to the reverse micellar solution of AOT in isooctane beyond a certain threshold concentration. The gel is very rigid and

stable at 1:1 AOT/*p*-chlorophenol ratios. Several equilibrium stages between the system of dry reverse micelles of AOT and a 1:1 AOT/*p*-chlorophenol (molar ratio) gel in isooctane have been examined by progressively adding *p*-chlorophenol to the dilute solutions of AOT in isooctane. This microstructural evolution has been studied through a combination of light scattering, small-angle neutron scattering (SANS), NMR, and rheology. The light scattering and the SANS data indicate that the dry micelles of AOT in isooctane do not undergo any detectable structural change up to a certain *p*-chlorophenol concentration. The rheological response of these systems corroborates this observation. NMR data show that the two components (AOT and *p*-chlorophenol) of the organogel interact, even though no structural change is observed in the AOT reverse micelles below this level of *p*-chlorophenol doping. Upon a very small increment in the concentration of *p*-chlorophenol beyond this “threshold” concentration, large aggregates are observed. An enhanced light and low-angle neutron scattering reflects the formation of these large aggregates. These aggregates are large enough to be detected by the naked eye. At this threshold concentration, these aggregates are freely floating in a pool of solvent. Optical microscopy reveals that these aggregates are composed of loosely entangled fibers, with poor interaggregate connectivity. The rheological response of this system is typical of pregels, supporting the findings. Above this threshold concentration, a well-developed three-dimensional network of fibers can be seen through optical microscopy. The rheological responses of these systems are in agreement with the behavior of cross-linked/entangled three-dimensional networks. The NMR data for these organogels indicate that the motion of the *p*-chlorophenol molecules in the network is restricted on the NMR time scale. This sharp transition indicates two possibilities: (i) a critical aggregation phenomenon that leads to the formation of large strands that entangle to form a viscoelastic three-dimensional network; (ii) a very narrow range of *p*-chlorophenol concentration in which structural changes in the reverse micelles of AOT take place.

**Acknowledgment.** We are grateful to Dr. Boualem Hammouda (NIST) for insightful discussions. Dr. Hammouda is also acknowledged for help in acquiring the SANS data. The National Institute of Standards and Technology, U.S. Department of Commerce, is gratefully acknowledged for providing the neutron research facilities used in this work through Grant NSF/DMR-9986442. This work was supported by grants from the National Science Foundation (Grants 9909912 and 0092001) and NASA (NAG-1-02070). Disclaimer: NIST does not endorse equipment or chemicals mentioned in this paper.

(45) Terech, P.; Pasquier, D.; Bordas, V.; Rossat, C. *Langmuir* **2000**, *16*, 4485.